

Can SMOS Data be Used Directly on the 15-km Discrete Global Grid?

Gift Dumedah, Jeffrey P. Walker, and Christoph Rüdiger, *Member, IEEE*

Abstract—Radiometric observations from the Soil Moisture and Ocean Salinity (SMOS) mission are processed to Level 1 brightness temperature (T_b) with ~ 42 -km spatial resolution and reported on a 15-km hexagonal Discrete Global Grid (DGG). While these data should be used at the 42-km resolution which the over-sampled DGG represents, this paper poses the question of whether they can be used directly at 15-km resolution without undertaking downscaling or implementing multiscale-type procedures when used in data assimilation. To assess the error associated with using the 42-km SMOS T_b data at 15-km resolution, this study employs 1-km T_b data from the Australian Airborne Cal/Val Experiment for SMOS (AACES). The study compares SMOS-like data derived from AACES at 42-km resolution with T_b values actually observed on the 15-km DGG. These 15-km DGG data are subsequently interpolated to a regular 12-km model grid and compared with actual observations at that resolution. The results show that the average root mean square differences in T_b between the 15- and 42-km footprints are 4.5 K and 3.9 K for horizontal (H) and vertical (V) polarizations, respectively, with a maximum difference of 12.9 K. The errors when interpolating the 42-km data onto the 12-km model grid were estimated to be 3.3 K for H polarization and 2.9 K for V polarization under the assumption of independence or 4.5 K and 3.9 K for H and V polarizations, respectively, with 4.0 K in H polarization and 3.6 K in V polarization from the 15- to 12-km interpolation process alone. An evaluation of the T_b differences for 42-km data assumed on the 15-km DGG found no correlation with vegetation based on leaf area index and only slight correlation with the spatial variance of SMOS data and topographic roughness. Given these differences and the noise that currently exists in SMOS T_b at 42 km, the 15-km DGG data can be used directly on the hexagonal grid or interpolated onto a regular grid of equivalent spatial resolution without further degrading the data quality.

Index Terms—Brightness temperature, Soil Moisture and Ocean Salinity (SMOS), soil moisture retrieval.

I. INTRODUCTION

THE Soil Moisture and Ocean Salinity (SMOS) mission is providing continuous L-band (1.4-GHz) radiometric measurements over the Earth surface at ~ 42 -km resolution with a repeat cycle of two to three days [1]. The brightness temperature (T_b) measurements are made at a range of incidence angles from 0° to 55° at vertical (V) and horizontal (H) polarizations. The synthetic aperture capability of SMOS

means that the T_b observations are processed and reported on the Icosahedral Snyder Equal Area projection (ISEA 4H9) which is a hexagonal grid called the Discrete Global Grid (DGG), with a spacing (spatial resolution) of about 15-km. This difference in spatial resolutions, 42-km for the actual T_b observation and 15-km for the reported T_b , pose soil moisture retrieval and data assimilation opportunities for land surface models that have spatial resolutions smaller than 42-km.

Ideally, the spatial resolution of retrieved soil moisture and the T_b values used in assimilation should be the same as the actual 42-km SMOS observation. However, a recurring question is whether the actual 42-km SMOS T_b observation can be used directly on the 15-km SMOS DGG, which has not yet been examined. Being able to use the SMOS data directly at the higher spatial resolution will circumvent the need for downscaling approaches such as those from [2] and [3], the need for a multiscale assimilation procedure such as [4], or data thinning to a regular 42-km grid. Otherwise, the overlapping characteristics of the DGG representation may need to be fully accounted for through a 3-D data assimilation scheme [5], [6]. These challenges add an extra layer of complexity and a source of uncertainty to the data assimilation procedure.

This study investigates whether the 42-km SMOS T_b observations may be used directly on the 15-km DGG that they are reported on and what the uncertainty implications would be due to differences in the two spatial resolutions. The estimated uncertainty resulting from the two spatial resolutions can facilitate the decision-making process of whether the 42-km resolution T_b can be used directly on the 15-km DGG for a particular application or not. The effect of interpolating to a chosen model grid with smaller spatial resolution is also assessed. These questions are addressed through the use of high-resolution T_b observations from the Australian Airborne Cal/Val Experiment for SMOS (AACES) [7]. The AACES data cover the Murrumbidgee Catchment in southeastern Australia with diverse climatic and varying physiographic conditions. The high-resolution AACES data offer the capability to explore the representativeness of T_b at a variety of spatial resolutions and thus determine the level of uncertainty associated with using T_b observations made at one resolution and applied at another. Specifically, the results quantify the level of uncertainty expected when applying the following: 1) 42-km SMOS T_b observations on the 15-km DGG and 2) the subsequent interpolation of this 15-km T_b representation to a 12-km model grid. The possibility to flag times and/or locations when larger than acceptable errors are expected is also examined using three factors: 1) spatial variance of SMOS Level 1 observations; 2) density of vegetation cover; and 3) topography.

Manuscript received November 10, 2012; revised March 8, 2013; accepted April 5, 2013. This work was supported by the Australian Research Council under Grant DP0879212.

The authors are with the Department of Civil Engineering, Monash University, Melbourne, Vic. 3800, Australia (e-mail: dgiftman@hotmail.com; jeff.walker@monash.edu; chris.rudiger@monash.edu).

Color versions of one or more of the figures in this paper are available online at <http://ieeexplore.ieee.org>.

Digital Object Identifier 10.1109/TGRS.2013.2262501

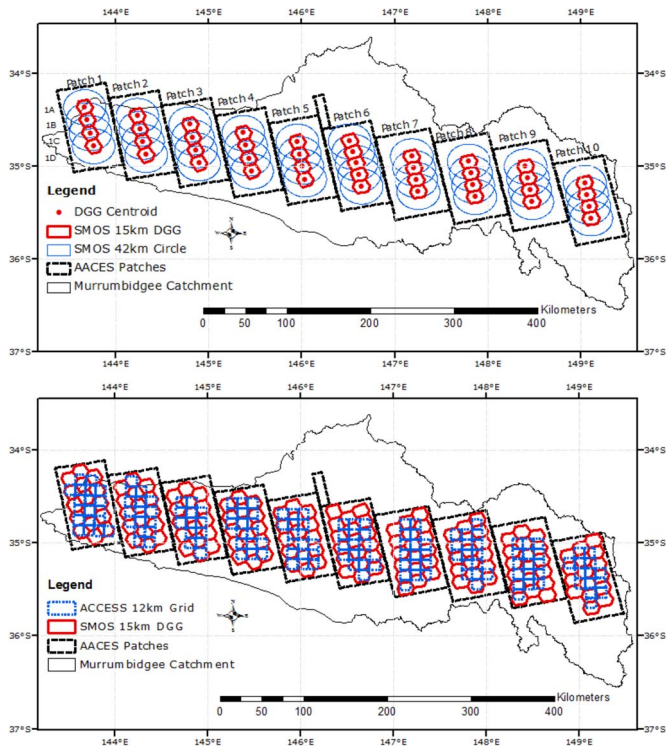


Fig. 1. Murrumbidgee Catchment study area showing the ACES flight patches, the SMOS 15-km DGG, and 42-km footprints (circles) that they represent. The bottom panel also shows the 12-km ACCESS model grid. Flight patch numbering starts with 1 at the left to 10 at the right. The DGG is labeled according to the flight patch number and alphabetic character starting with “A” at the top grid to “D” at the bottom grid except for patch 6 whose bottom grid is “E.”

II. MATERIALS AND METHODS

A. Study Area and T_b Data

The 80 000-km² Murrumbidgee Catchment shown in Fig. 1 has varied climatic, topographic, and land-cover characteristics with semi-arid conditions in the west to alpine conditions (including wintertime snow) in the east. The ACES campaign was undertaken in 2010 across the Murrumbidgee Catchment including ACES-1 in the summer and ACES-2 in the winter [7]. ACES-1 commenced on January 18 and was completed on February 21, whereas ACES-2 was undertaken from September 8 to 26. The airborne radiometer data cover a 500 × 100 km² area which is composed of the ten flight patches shown in Fig. 1, each being 50 × 100 km². The flight patches are aligned with the SMOS 15-km DGG; each patch contains a minimum of four overlapping SMOS pixels of about 42-km resolution. The microwave radiometer used is the Polarimetric L-band Multibeam Radiometer (PLMR) at 1.413-GHz frequency (the same frequency as in SMOS), which was mounted such that it scanned the surface at three incidence angles of ±7°, ±21.5°, and ±38.5° to each side of the aircraft. The PLMR used to make the 1-km T_b observations has an accuracy better than 2 K with sensitivity better than 1 K [8]. As a result, the uncertainty associated with the 1-km ACES T_b is taken to be 2 K.

The ACES data used in this study include the 1-km L-band T_b data normalized to a common 38° incidence angle to simulate a single incidence angle of SMOS Level 1 T_b

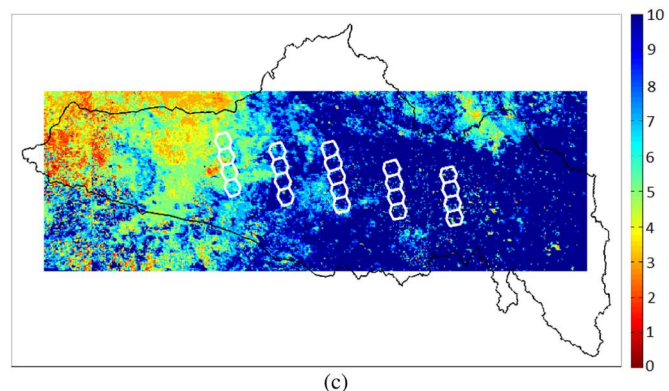
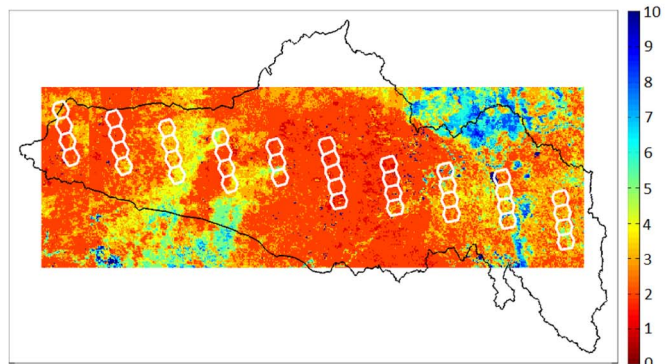
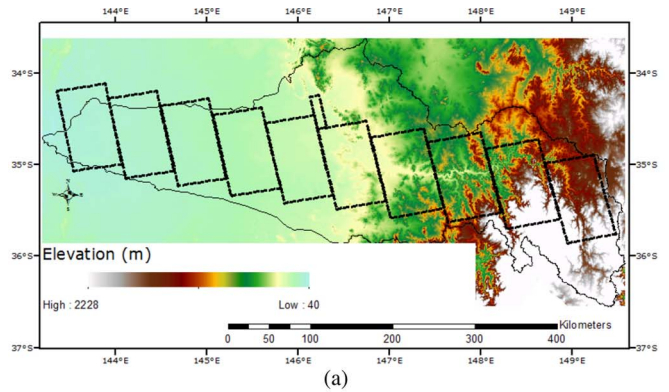


Fig. 2. Topographic information and density of vegetation cover in the Murrumbidgee Catchment during ACES observations (data source: DEM—Geoscience Australia; MODIS LAI-NASA LP DAAC at https://lpdaac.usgs.gov/get_data). (a) Terrain elevation showing smooth topographic roughness in the west to high topographic roughness in the east. (b) MODIS LAI in square meters per square meter during ACES-1 from January 18 to February 21. (c) MODIS LAI in square meters per square meter during ACES-2 from September 8 to 26.

data. The actual SMOS Level 1 T_b observations at about 38° incidence angle are only used in this study to examine the spatial variability of T_b as represented by SMOS data on the DGG within a single SMOS footprint. The reason for this reliance on the ACES data is the high resolution that it affords, allowing the questions of spatial resolution and interpolation to be fully addressed.

B. Topography and Vegetation Cover

The topography and the density of vegetation cover in the Murrumbidgee Catchment are shown in Fig. 2. The topography is represented through digital elevation model (DEM) data,

obtained from Geoscience Australia through the GEODATA 9 Second DEM (DEM-9S) Version 3 in 2008. The DEM has a spatial resolution of 250 m with a positional accuracy (in nominal scale) of 1:250 000. The topography in AACES patches 1–5 is flat, indicating low topographic roughness with patch 6 having gently sloping terrain and patches 7–10 have undulating terrain indicative of high topographic roughness. The density of vegetation cover is approximated using leaf area index (LAI) data in square meters per square meter from the 1-km Moderate-Resolution Imaging Spectroradiometer (MODIS) data. The LAI information on January 25 and September 13, 2010 are used to represent the density of vegetation cover during the AACES-1 and AACES-2 observation periods, respectively. Generally, the density of vegetation cover is less during AACES-1 compared with that during the AACES-2 observation period. The density of vegetation cover is highest at the eastern portion of the catchment, which comprises conservation areas and state forests, whereas the western areas are characterized mainly with grassland. It is noteworthy that the moderate densities of vegetation cover during AACES-1 around patches 3–4 in the central portion of the catchment are cropping irrigation areas.

C. Application Methods

The evaluation of T_b observations for the two spatial resolutions and interpolation onto a model grid is divided into three parts: A, B, and C. Part A examines the differences in T_b when 1-km AACES data are aggregated according to the 15-km DGG as compared with the 1-km AACES data aggregated for the actual 42-km footprint that it represents. Hereafter, the 1-km AACES data are denoted as $T_b^{1 \text{ km}}$, the aggregations to 15-km DGG as $T_b^{15 \text{ km}}$, the aggregations to 42 km as $T_b^{42 \text{ km}}$, and the use of $T_b^{42 \text{ km}}$ data as if they were the true $T_b^{15 \text{ km}}$ values as $T_b^{42/15 \text{ km}}$. The aggregations are performed by finding the average of all $T_b^{1 \text{ km}}$ grids that are contained within each of the 15-km DGG using (1) and in the actual 42-km SMOS footprint according to (2). The associated uncertainties for $T_b^{15 \text{ km}}$ and $T_b^{42 \text{ km}}$ are estimated using (3) and (4), respectively, derived according to the standard error propagation procedure [9] under the assumption that the error of each measurement is independent. This assumption is appropriate, given the nature of the errors in individual PLMR measurements and the application of the T_b data herein

$$T_b^{15 \text{ km}} = \frac{\sum_{i=1}^k T_{b,i}^{1 \text{ km}}}{k} \quad (1)$$

where k is the number of 1-km grids within the 15-km grid

$$T_b^{42 \text{ km}} = \frac{\sum_{i=1}^n T_{b,i}^{1 \text{ km}}}{n} \quad (2)$$

where n is the number of 1-km grids within the 42-km grid

$$\sigma_{T_b^{15 \text{ km}}} = \sqrt{\sum_{i=1}^k \left(\frac{\sigma_{T_{b,i}^{1 \text{ km}}}^2}{k^2} \right)} \quad (3)$$

where $\sigma_{T_b^{1 \text{ km}}}$ is the uncertainty from the 1-km T_b ($\approx 2 \text{ K}$)

$$\sigma_{T_b^{42 \text{ km}}} = \sqrt{\sum_{i=1}^n \left(\frac{\sigma_{T_{b,i}^{1 \text{ km}}}^2}{n^2} \right)}. \quad (4)$$

Using $T_b^{15 \text{ km}}$ for the 15-km DGG and $T_b^{42 \text{ km}}$ for the actual 42-km SMOS footprint, the differences in T_b between the two spatial resolutions provide an estimate of the uncertainty when applying the 42-km SMOS data directly on the 15-km DGG as $T_b^{42/15 \text{ km}}$. The absolute difference in T_b between the 15-km DGG and the actual 42-km SMOS footprint, referred to hereafter as T_b^{42-15} , is estimated in (5) and the associated uncertainty of this difference, denoted as $\sigma_{T_b^{42-15}}$, is determined according to (6)

$$T_b^{42-15} = |T_b^{42 \text{ km}} - T_b^{15 \text{ km}}| \quad (5)$$

$$\sigma_{T_b^{42-15}} = \sqrt{(\sigma_{T_b^{42 \text{ km}}})^2 + (\sigma_{T_b^{15 \text{ km}}})^2}. \quad (6)$$

The rationale of this evaluation is to determine the level of uncertainty in T_b when the actual 42-km SMOS observations are approximated to the 15-km DGG. Knowledge of the uncertainty in $T_b^{42/15 \text{ km}}$ will potentially allow practitioners to use the 42-km SMOS T_b observations directly at the 15-km DGG.

Part B assesses the uncertainty when interpolating the 15-km DGG T_b to model grids with geometry and resolution that are different to the DGG or the data-thinned original 42-km resolution. The model grid used in this study is a 12-km square grid which represents the numerical weather prediction grid from the Australian Community Climate and Earth-System Simulator (ACCESS). Consequently, two estimates of T_b are required for the 12-km model grid: one as a direct aggregation of the 1-km AACES data onto the 12-km resolution, hereafter referred to as $T_b^{12 \text{ km}}$, and the other as a weighted sum of the 15-km DGG T_b according to the areal overlaps with the 12-km resolution, hereafter referred to as $T_b^{w12 \text{ km}}$. The aggregated estimate $T_b^{12 \text{ km}}$ is determined by finding the average of the 1-km AACES data that are contained within the 12-km grid according to (7) with its associated uncertainty $\sigma_{T_b^{12 \text{ km}}}$ in (8) under the assumption of independence

$$T_b^{12 \text{ km}} = \frac{\sum_{i=1}^m T_{b,i}^{1 \text{ km}}}{m} \quad (7)$$

where m is the number of 1-km grids within the 12-km grid

$$\sigma_{T_b^{12 \text{ km}}} = \sqrt{\sum_{i=1}^m \left(\frac{\sigma_{T_{b,i}^{1 \text{ km}}}^2}{m^2} \right)} \quad (8)$$

where $\sigma_{T_b^{1 \text{ km}}}$ is the uncertainty from the 1-km T_b .

Since the PLMR coverage is not sufficiently large to provide the $T_b^{42/15 \text{ km}}$ values required by the 15-km DGG represented in the bottom panel of Fig. 1, only the actual 15-km DGG observations $T_b^{15 \text{ km}}$ could be used for explicit representation of the DGG and thus provide an estimate of $T_b^{12 \text{ km}}$ (denoted as $*T_b^{w12 \text{ km}}$) when using (9). While the difference between these two values ($T_b^{12 \text{ km}}$ and $*T_b^{w12 \text{ km}}$) provides an estimate of the error from interpolation itself and not the scaling error

that comes from using SMOS data directly on the DGG; error propagation on the interpolation equation in (9) will provide the theoretical error estimate.

The weighted 12-km estimate $*T_b^{w12 \text{ km}}$ is calculated according to (9) as a weighted sum by area (in terms of fractional coverage) for each 12-km grid using the 42-km observation on the 15-km grid [$T_b^{42/15 \text{ km}}$ from (2)]. The corresponding uncertainty estimate for $*T_b^{w12 \text{ km}}$ denoted as $*\sigma_{T_b^{w12 \text{ km}}}$ is estimated according to (10) from the standard error propagation procedure [9]. The estimate of the error from applying 42-km observations at 15-km DGG resolution, denoted as $\sigma_{T_b^{42/15 \text{ km}}}$, is taken as the root mean square difference (RMSD) for the difference calculated in (5)

$$*T_b^{w12 \text{ km}} = \sum_{i=1}^p \left(w_i * T_{b,i}^{42/15 \text{ km}} \right) \quad (9)$$

where p is the number of 15-km grids which overlap the 12-km grid, $w = A_{15 \text{ km}}^*/A_{12 \text{ km}}$, $A_{15 \text{ km}}^*$ is the area of the 15-km grid which overlaps with the 12-km grid, and $A_{12 \text{ km}}$ is the total area of the 12-km grid

$$*\sigma_{T_b^{w12 \text{ km}}} = \sqrt{\sum_{i=1}^m \left(w_i^2 * \sigma_{T_{b,i}^{42/15 \text{ km}}}^2 \right)}. \quad (10)$$

The weighted 12-km estimate and its error estimate from the actual 15-km data, denoted as $*T_b^{w12 \text{ km}}$, can be calculated from (9) and (10) by using $T_b^{15 \text{ km}}$ in place of $T_b^{42/15 \text{ km}}$ and $\sigma_{T_b^{15 \text{ km}}}$ from (3) in place of $\sigma_{T_b^{42/15 \text{ km}}}$.

Part C is an attempt to identify when and/or where it is more appropriate to approximate the 42-km SMOS T_b data on the 15-km DGG. This includes an evaluation of the differences in T_b between the observed 15-km resolution and the actual observation at 42 km in comparison with three factors: 1) the spatial variance of SMOS Level 1 data, 2) the density of vegetation cover, and 3) topographic roughness. The spatial variance of SMOS data is determined for each 15-km DGG by using its T_b value and the values from neighboring DGGs which fall within the 42-km SMOS footprint. The computed variance of T_b provides a measure of variability for the overlapping SMOS observations. The density of vegetation cover is represented using MODIS LAI by finding the average of all the 1-km LAI within each of the 42-km SMOS pixels.

The topographic roughness for each of the 42-km SMOS pixels is estimated using the DEM data. The derived terrain slope angles from the DEM were used to estimate a topographic indicator as an absolute value of the product of spatial variance and skewness of the slope angle. This topographical indicator is denoted as $sVar$ and provides an index of both the heterogeneity (variance) and uniformity (skewness) of the landscape [10]. It is noteworthy that $sVar$ is a relative measure that is meaningful only for a particular defined area. High values of $sVar$ indicate that the terrain is nonuniformly heterogeneous, low values mean a uniformly homogeneous terrain, and moderate values mean that the terrain is either uniformly heterogeneous or nonuniformly homogeneous. These comparisons are aimed to determine whether the pattern of uncertainty found between

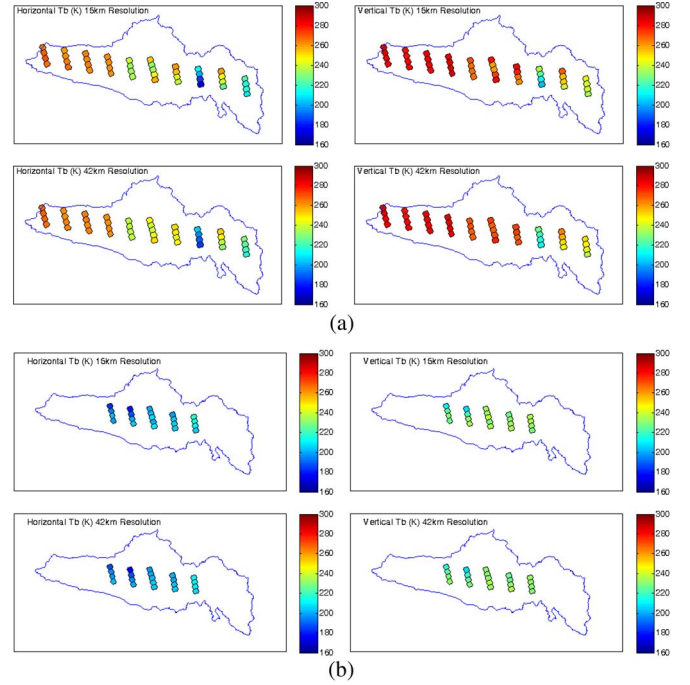


Fig. 3. Brightness temperature in kelvin; observed 1-km AACES T_b aggregated to the 15-km DGG and to the actual 42-km SMOS footprint that is represented on the 15-km DGG. (a) AACES-1: Patch numbering starts from 1 at far left to 10 at far right. (b) AACES-2: Patch numbering starts from 4 at far left to 8 at far right.

the 15-km DGG representation and the actual 42-km SMOS footprint corresponds to the spatial variability in the SMOS data, vegetation cover, or topographic roughness.

III. RESULTS AND DISCUSSION

A. Variability of Aggregated T_b for Actual 42-km SMOS Footprint and 15-km DGG

The aggregated T_b values for the 15- and 42-km resolutions are presented in Fig. 3 for AACES-1 and AACES-2. In AACES-1, larger differences between the two resolutions can be seen in patches 8–10 (relatively wet conditions) whereas the remaining patches show little discernible differences for H and V polarizations. In AACES-2, the T_b differences for the two resolutions are minimal and limited to a few DGG pixels in both polarizations. It is noteworthy that in AACES-1, surface soil moisture obtained from *in situ* point observations varied considerably from dry conditions of $0.05\text{--}0.10 \text{ m}^3/\text{m}^3$ for the left patches (1–4) to wet conditions of $0.25\text{--}0.35 \text{ m}^3/\text{m}^3$ for the right patches (5–10), whereas consistent wet conditions of $0.2\text{--}0.4 \text{ m}^3/\text{m}^3$ persisted for all patches observed during AACES-2 [7].

The overall quantitative comparison between the two resolutions is shown in Fig. 4. Note that T_b values are generally low for AACES-2, reflecting the wetter conditions and lower surface temperatures prevailing during this winter campaign, whereas AACES-1 has values spread over the entire interval, reflecting the more varied soil moisture conditions. However, the pattern of differences in T_b between the two resolutions is similar for AACES-1 and AACES-2, as evidenced by their RMSD and R^2 . The RMSD between the two T_b estimates is 4.5 K in the H polarization and 3.9 K in the V polarization.

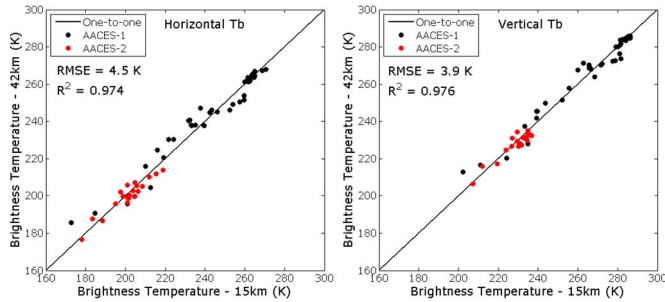


Fig. 4. Comparison between the aggregated T_b at 15- and 42-km resolutions, as shown in Fig. 3. The estimated T_b errors according to (3) and (4) are 0.2 K for $T_b^{15\text{ km}}$ and 0.1 K for $T_b^{42\text{ km}}$ under the assumption of independence. If dependence was assumed, then these would each increase to the original 2-K uncertainty of PLMR.

While the results show that the highest T_b values, indicative of extreme dry locations, have an almost perfect match between the two resolutions in both polarizations, the T_b comparison between the two resolutions does not significantly degrade for T_b values. Thus, the T_b differences shown here do not seem to be strongly correlated with soil moisture (dry or wet). Rather, the closer agreement at the extreme dry locations is, in general, due to the homogeneous nature (e.g., vegetation cover and physiographic heterogeneity) of the landscape, together with uniform soil moisture conditions over large areas. The terrain and vegetation density are much more heterogeneous in the eastern portion of the catchment, indicating that these locations are likely to have more dynamic and nonuniform moisture conditions. As will be shown later, the lowest absolute differences in T_b between the two resolutions are all located in patches 1–4, being the western portion of the catchment.

B. Variability of T_b Between Aggregated 12-km and Weighted 12-km Model Grids

The aggregated 12-km T_b and its weighted estimate using the observed 15-km T_b are shown in Fig. 5, with very little difference between the two T_b estimates for both polarizations across AACES-1 and AACES-2. The quantitative comparison for the two 12-km estimates is shown in Fig. 6. This confirms the similarity in pattern with a coefficient of determination (R^2) of about 0.98 in both polarizations. The RMSD value between the two T_b estimates is 4.0 K in the H polarization and 3.6 K in the V polarization. However, as noted earlier, this comparison only represents the error introduced by interpolating from the 15-km DGG to the 12-km grid and does not account for the error of SMOS data representation on the 15-km DGG. Due to the limitations of the available data set, this can only be estimated from error proration calculation and not by direct deduction.

By using the RMSD values from Part A as estimates of uncertainty in the T_b data on the 15-km DGG (i.e., $\sigma_{T_b^{42/15}}$), the overall uncertainty in T_b associated with interpolating the 42-km SMOS data to the 12-km model grid can be calculated from (10) as 3.3 K in the H polarization and 2.9 K in the V polarization under the assumption of independence. However, under the assumption of dependence, the uncertainty estimates would remain as 4.5 K in the H polarization and 3.9 K in the V polarization. Alternatively, assuming additive errors, the error in interpolating the 42-km SMOS data onto the 12-km grid can

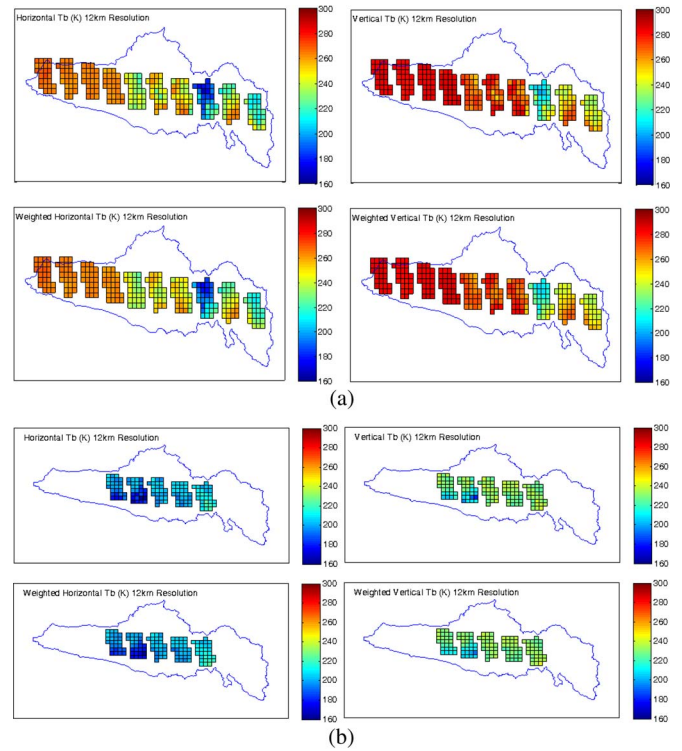


Fig. 5. Brightness temperature in kelvin; observed 1-km AACES T_b aggregated to the 12-km model grid and the weighted 12-km T_b estimated as the weighted sum of 15-km T_b as in Fig. 3. (a) AACES-1: Patch numbering starts from 1 at far left to 10 at far right. (b) AACES-2: Patch numbering starts from 4 at far left to 8 at far right.

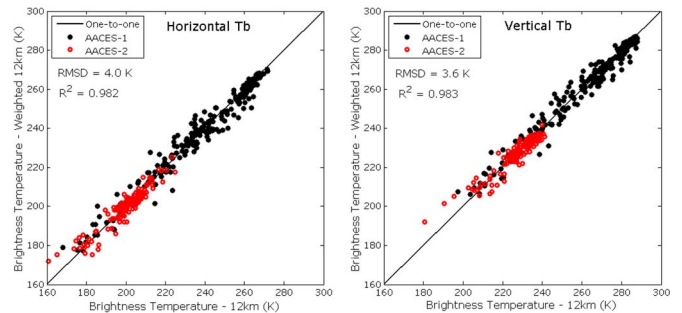


Fig. 6. Comparison between observed 1-km AACES T_b aggregated to the 12-km T_b and the weighted 12-km T_b estimated as the weighted sum of aggregated 15-km T_b , as shown in Fig. 5. The associated T_b errors according to (8) and (10) (using $T_b^{15\text{ km}}$) are 0.2 K for $T_b^{12\text{ km}}$ and 1.8 K for $T_b^{w12\text{ km}}$ under the assumption of independence. If dependence was assumed, then these would each increase to the original 2-K uncertainty of PLMR.

be estimated as $\sqrt{(4.5)^2 + (4.0)^2} = 6.0$ K in the H polarization and $\sqrt{(3.9)^2 + (3.6)^2} = 5.3$ K in the V polarization.

C. Indicators for Estimating T_b Differences Between 15- and 42-km Resolutions

This section presents the differences in T_b between the 15-km DGG and the 42-km SMOS footprint in comparison with the three indicators: spatial variance of SMOS Level 1 data, vegetation cover, and topography. Using T_b differences between the 15- and 42-km resolutions, the spatial variance of actual SMOS observations are compared with the absolute differences from Part A. The variance for each SMOS DGG is computed by finding the standard deviation of T_b using values from the

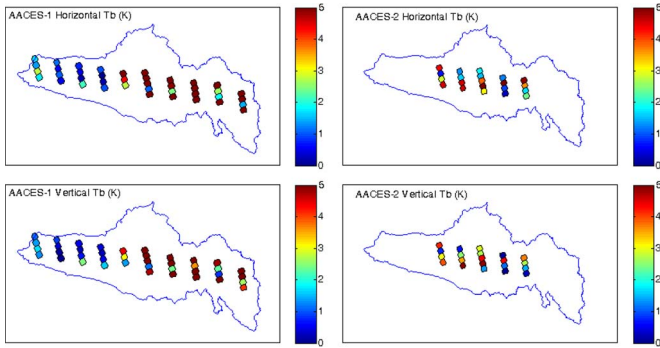


Fig. 7. Brightness temperature in kelvin; absolute difference of T_b between observed 1-km AACES T_b aggregated to the 42-km SMOS footprint and the actual observations for the 15-km DGG, as shown in Fig. 3.

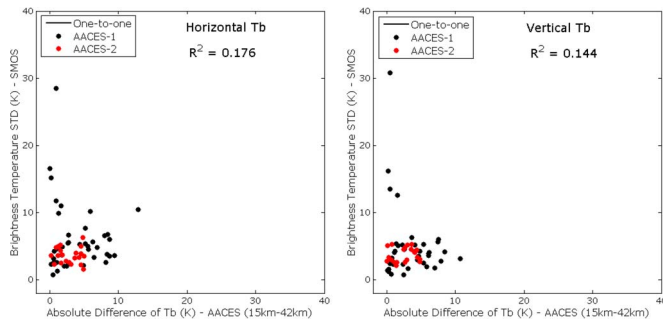


Fig. 8. Comparison between standard deviation of actual SMOS T_b observations within a given footprint and the absolute difference of T_b shown in Fig. 7. The R^2 values are computed after removing SMOS standard deviation and AACES absolute values greater than 10 K.

footprint in question and the six other neighboring DGG values that fall within it. This comparison of the actual T_b standard deviation with the absolute difference provides a mechanism to determine if any relationship exists to identify places and/or times when the difference in T_b is expected to exceed a given tolerance. The absolute difference of T_b between the 42- and 15-km resolutions is shown in Fig. 7.

Generally, the smaller absolute differences occur in patches 1–4 in the western portion of the catchment, as shown previously to have smooth topographical roughness. The figure identifies (by deep brown shading) grids with absolute differences greater than the overall RMSD values of 4.6 K for H polarization and 3.9 K for V polarization in Part A; note that the grid labels have been defined earlier in Fig. 1. These grids (in patches 5–10) are generally located in the eastern portion having heterogeneous physiographic conditions of the catchment. The grids in patches 7 and 8 (e.g., 7B and 8A) have consistently high absolute differences for both V and H polarizations in AACES-1 and AACES-2. Patches 9 and 10 also have high absolute differences in V and H polarizations in AACES-1. The persistent pattern in these grids suggests that they are associated with unique physiographic/observation features.

The computed standard deviation using actual SMOS Level 1 T_b for the grids are compared with the T_b absolute difference in Fig. 8 for both H and V polarizations. The estimated standard deviation values are generally below 10 K, but four isolated grids have high variance values ranging from above 10 K to 30 K. These high standard deviation values are generally found in patch 4, which has extensive but scattered crop irrigation ar-

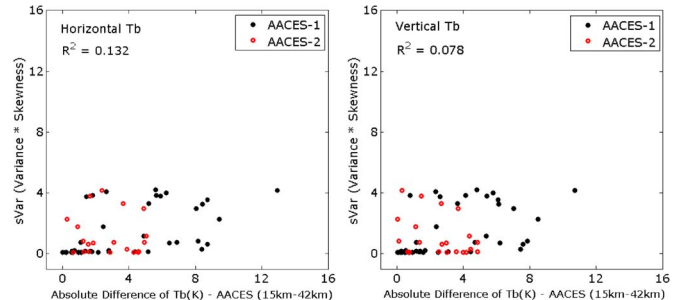


Fig. 9. Comparison between topographical roughness $sVar$ and the absolute difference of T_b shown in Fig. 7.

eas. The overall pattern of the T_b standard deviation is unrelated to dry or wet locations in the Murrumbidgee Catchment. Based on the R^2 values, there is only a weak relationship between the standard deviation of SMOS Level 1 T_b and the absolute difference computed using 42- and 15-km resolutions.

The absolute difference of T_b for the two resolutions was also examined in relation to topographic roughness and vegetation cover using LAI. It was found from the LAI data that there are different densities of vegetation cover during the two field campaigns, yet the absolute differences of T_b are similar for the two seasons. As a result, the absolute differences in T_b between the 15-km DGG and actual 42-km SMOS footprint do not correlate to the density of vegetation cover.

For topography, the varied terrain pattern indicative of high topographic roughness at the eastern portion of the Murrumbidgee Catchment is consistent with the high absolute differences of T_b in patches 5–10. The impact of topography is examined by comparing the topographical index $sVar$ with the absolute differences of T_b in Fig. 9. The $sVar$ pattern shows a weak relationship (based on the R^2 values) with the absolute differences of T_b in both H and V polarizations.

Overall, the topography, vegetation, and spatial variance of SMOS Level 1 data show weak relationships to the absolute differences in T_b . Given these findings, none of the three indicators evaluated was able to identify where (i.e., spatial locations) and when (e.g., days or seasons) the differences in T_b for 15- and 42-km resolutions will be large or small.

IV. CONCLUSION

This study has applied 1-km T_b data from AACES to examine the potential error from using the 15-km DGG to represent T_b observations at the actual 42-km SMOS footprint and subsequent interpolation to a 12-km model grid. The evaluation shows that the overall differences in T_b based on RMSD between the 15-km DGG and the actual 42-km footprint are about 4.5 K and 3.9 K for H and V polarizations, respectively. The pattern of differences in T_b show that larger absolute differences were associated with heterogeneous physiographic areas whereas smaller differences were related to homogeneous areas with low topographic roughness of the catchment. As a result, the differences in T_b were further examined in relation to three features: the spatial variance of SMOS Level 1 data, vegetation cover, and topographic roughness. However, only poor relationships were found with these three indicator variables.

When interpolating SMOS T_b data from the 15-km DGG to a 12-km regular grid, results showed that the overall differences in T_b between aggregated 12-km and weighted 12-km from the 15-km observation were 4.0 K and 3.6 K for H and V polarizations, respectively. By taking into account the T_b error in representing the 42-km SMOS footprint directly on the 15-km DGG, together with the interpolation from the 12-km resolution, the overall error from 42- to 12-km resolution was estimated to be between 3.3 K and 4.5 K in the H polarization and between 2.9 K and 3.9 K in the V polarization according to the assumption made in relation to dependence. The independent combination of the T_b errors associated with the two interpolations shows T_b uncertainties of 6 K and 5.3 K in the H and V polarizations, respectively.

This evaluation of differences in T_b between the actual 42-km footprint and the 15-km DGG provides an estimate of the uncertainty to be expected for similar physiographic regions when applying SMOS data directly on the DGG. Given the estimated errors, the SMOS T_b observations at 42 km can be used directly on the DGG without downscaling procedures, as the expected RMSD is not worse than the noise that currently exists in SMOS T_b measurements. That is, soil moisture retrieval and data assimilation applications can use the 42-km SMOS T_b observations on the 15-km DGG without downscaling since the estimated errors in T_b between the two resolutions are smaller than the standard error of the current SMOS T_b data.

ACKNOWLEDGMENT

The authors would like to thank all participants in both AACES campaigns, the anonymous reviewers for their comments, and the Editor for handling the manuscript.

REFERENCES

- [1] Y. Kerr, P. Waldteufel, J.-P. Wigneron, S. Delwart, F. Cabot, J. Boutin, M.-J. Escorihuela, J. Font, N. Reul, C. Gruhier, S. Juglea, M. Drinkwater, A. Hahne, M. Martin-Neira, and S. Mecklenburg, "The SMOS mission: New tool for monitoring key elements of the global water cycle," *Proc. IEEE*, vol. 98, no. 5, pp. 666–687, May 2010.
- [2] O. Merlin, C. Rüdiger, A. Al Bitar, P. Richaume, J. Walker, and Y. Kerr, "Disaggregation of SMOS soil moisture in Southeastern Australia," *IEEE Trans. Geosci. Remote Sens.*, vol. 50, no. 5, pp. 1556–1571, May 2012.
- [3] M. Piles, A. Camps, M. Vall-llossera, I. Corbella, R. Panciera, C. Rüdiger, Y. Kerr, and J. Walker, "Downscaling SMOS-derived soil moisture using MODIS visible/infrared data," *IEEE Trans. Geosci. Remote Sens.*, vol. 49, no. 9, pp. 3156–3166, Sep. 2011.
- [4] M. Pan and E. F. Wood, "Impact of accuracy, spatial availability, and revisit time of satellite-derived surface soil moisture in a multiscale ensemble data assimilation system," *IEEE J. Sel. Topics Appl. Earth Observ. Remote Sens.*, vol. 3, no. 1, pp. 49–56, Mar. 2010.
- [5] W. T. Crow and D. Ryu, "A new data assimilation approach for improving runoff prediction using remotely-sensed soil moisture retrievals," *Hydrol. Earth Syst. Sci.*, vol. 13, no. 1, pp. 1–16, Jan. 2009.
- [6] R. H. Reichle, W. T. Crow, R. D. Koster, H. O. Sharif, and S. P. P. Mahanama, "Contribution of soil moisture retrievals to land data assimilation products," *Geophys. Res. Lett.*, vol. 35, no. 1, p. L01 404, Jan. 2008.
- [7] S. Peischl, J. P. Walker, C. Rüdiger, N. Ye, Y. H. Kerr, E. Kim, R. Bandara, and M. Allahmoradi, "The AACES field experiments: SMOS calibration and validation across the Murrumbidgee River catchment," *Hydrol. Earth Syst. Sci.*, vol. 16, no. 6, pp. 1697–1708, Jun. 2012.
- [8] J. P. Grant, A. A. Van de Griend, J.-P. Wigneron, K. Saleh, R. Panciera, and J. P. Walker, "Influence of forest cover fraction on L-band soil moisture retrievals from heterogeneous pixels using multi-angular observations," *Remote Sens. Environ.*, vol. 114, no. 5, pp. 1026–1037, May 2010.
- [9] P. Fornasini, *The Uncertainty in Physical Measurements: An Introduction to Data Analysis in the Physics Laboratory*. New York, NY, USA: Springer-Verlag, 2008.
- [10] V. Guttal and C. Jayaprakash, "Spatial variance and spatial skewness: Leading indicators of regime shifts in spatial ecological systems," *Theor. Ecol.*, vol. 2, no. 1, pp. 3–12, Mar. 2009.



Gift Dumedah received the B.Sc. degree (with honors) in geodetic engineering from Kwame Nkrumah University of Science and Technology, Kumasi, Ghana, in 2002 with his thesis entitled "A Geographical Information System for the Ghana Army." He also received the M.Sc. degree in geography from Simon Fraser University, Vancouver, BC, Canada, in 2005, with a specialization in geographic information science, and the Ph.D. degree in geography from the University of Guelph, Guelph, ON, Canada, in 2010, with his thesis titled "Multi-Objective

Calibration of Hydrological Models and Data Assimilation Using Genetic Algorithms."

After his studies, he held a postdoctoral fellowship at the School of Geography and Earth Sciences, McMaster University, Hamilton, ON, Canada. In October 2011, he joined the Department of Civil Engineering, Monash University, Melbourne, Australia, where he is currently contributing to soil moisture research for sustainable land and water management. His research focus is on the integrated assessment of climate variability and human impact on sustainable water resources by employing advanced land surface monitoring strategies for efficient observation–model synthesis. His specific primary interests include observation–model synthesis, data assimilation, evolutionary computation, and remote sensing and GIScience applied to water resources.

Jeffrey P. Walker received the B.E. degree (with Honours 1 and University Medal) in civil engineering and B.S. degree in surveying (with Honours 1 and University Medal) and the Ph.D. degree in water resources engineering from The University of Newcastle, Newcastle, Australia, in 1995 and 1999, respectively. His Ph.D. thesis was among the early pioneering research on estimation of root-zone soil moisture from remotely sensed surface soil moisture observations.

He then joined the NASA Goddard Space Flight Center to implement his soil moisture work globally. In 2001, he moved to the Department of Civil and Environmental Engineering, The University of Melbourne, Melbourne, Australia, as a Lecturer, where he continued his soil moisture work, including the development of the only Australian airborne capability for simulating new satellite missions for soil moisture. Since 2010, he has been a Professor with the Department of Civil Engineering, Faculty of Engineering, Monash University, Melbourne, where he is continuing his research. He is contributing to soil moisture satellite missions at NASA, the European Space Agency, and JAXA as a Science Definition Team Member for the Soil Moisture Active Passive Mission and a Calibration/Validation Team Member for the Soil Moisture and Ocean Salinity mission.

Christoph Rüdiger (M'10) received the B.E. degree in civil engineering from the University of Applied Sciences of Wiesbaden, Wiesbaden, Germany, in 2002 and the Ph.D. degree in environmental engineering from The University of Melbourne, Melbourne, Australia, in 2007. His undergraduate thesis covered the topic of groundwater and contaminant flow around future buildings. His Ph.D. thesis was on the potential to assimilate streamflow data into land surface models for soil moisture prediction.

He then joined the Centre National de Recherches Météorologiques, Météo, Toulouse, France, where he worked on the preparation of surface soil moisture and leaf-area-index data assimilation into the French land surface model ISBA. During this period, he also worked on the validation of different passive and active microwave satellite products over France with a particular focus on Soil Moisture and Ocean Salinity (SMOS). Since his return to Australia in July 2008, he has coordinated and led a number of calibration/validation (cal/val) campaigns for the Australian land validation segment of European Space Agency's SMOS mission in the Australian arid zone and the Murrumbidgee River catchment. In addition to this, he continues to work on land surface data assimilation and also participates in the Australian cal/val campaigns for the Soil Moisture Active Passive and the Aquarius missions. He is currently with Monash University, Melbourne.

Can SMOS Data be Used Directly on the 15-km Discrete Global Grid?

Gift Dumedah, Jeffrey P. Walker, and Christoph Rüdiger, *Member, IEEE*

Abstract—Radiometric observations from the Soil Moisture and Ocean Salinity (SMOS) mission are processed to Level 1 brightness temperature (T_b) with ~ 42 -km spatial resolution and reported on a 15-km hexagonal Discrete Global Grid (DGG). While these data should be used at the 42-km resolution which the over-sampled DGG represents, this paper poses the question of whether they can be used directly at 15-km resolution without undertaking downscaling or implementing multiscale-type procedures when used in data assimilation. To assess the error associated with using the 42-km SMOS T_b data at 15-km resolution, this study employs 1-km T_b data from the Australian Airborne Cal/Val Experiment for SMOS (AACES). The study compares SMOS-like data derived from AACES at 42-km resolution with T_b values actually observed on the 15-km DGG. These 15-km DGG data are subsequently interpolated to a regular 12-km model grid and compared with actual observations at that resolution. The results show that the average root mean square differences in T_b between the 15- and 42-km footprints are 4.5 K and 3.9 K for horizontal (H) and vertical (V) polarizations, respectively, with a maximum difference of 12.9 K. The errors when interpolating the 42-km data onto the 12-km model grid were estimated to be 3.3 K for H polarization and 2.9 K for V polarization under the assumption of independence or 4.5 K and 3.9 K for H and V polarizations, respectively, with 4.0 K in H polarization and 3.6 K in V polarization from the 15- to 12-km interpolation process alone. An evaluation of the T_b differences for 42-km data assumed on the 15-km DGG found no correlation with vegetation based on leaf area index and only slight correlation with the spatial variance of SMOS data and topographic roughness. Given these differences and the noise that currently exists in SMOS T_b at 42 km, the 15-km DGG data can be used directly on the hexagonal grid or interpolated onto a regular grid of equivalent spatial resolution without further degrading the data quality.

Index Terms—Brightness temperature, Soil Moisture and Ocean Salinity (SMOS), soil moisture retrieval.

I. INTRODUCTION

THE Soil Moisture and Ocean Salinity (SMOS) mission is providing continuous L-band (1.4-GHz) radiometric measurements over the Earth surface at ~ 42 -km resolution with a repeat cycle of two to three days [1]. The brightness temperature (T_b) measurements are made at a range of incidence angles from 0° to 55° at vertical (V) and horizontal (H) polarizations. The synthetic aperture capability of SMOS

means that the T_b observations are processed and reported on the Icosahedral Snyder Equal Area projection (ISEA 4H9) which is a hexagonal grid called the Discrete Global Grid (DGG), with a spacing (spatial resolution) of about 15-km. This difference in spatial resolutions, 42-km for the actual T_b observation and 15-km for the reported T_b , pose soil moisture retrieval and data assimilation opportunities for land surface models that have spatial resolutions smaller than 42-km.

Ideally, the spatial resolution of retrieved soil moisture and the T_b values used in assimilation should be the same as the actual 42-km SMOS observation. However, a recurring question is whether the actual 42-km SMOS T_b observation can be used directly on the 15-km SMOS DGG, which has not yet been examined. Being able to use the SMOS data directly at the higher spatial resolution will circumvent the need for downscaling approaches such as those from [2] and [3], the need for a multiscale assimilation procedure such as [4], or data thinning to a regular 42-km grid. Otherwise, the overlapping characteristics of the DGG representation may need to be fully accounted for through a 3-D data assimilation scheme [5], [6]. These challenges add an extra layer of complexity and a source of uncertainty to the data assimilation procedure.

This study investigates whether the 42-km SMOS T_b observations may be used directly on the 15-km DGG that they are reported on and what the uncertainty implications would be due to differences in the two spatial resolutions. The estimated uncertainty resulting from the two spatial resolutions can facilitate the decision-making process of whether the 42-km resolution T_b can be used directly on the 15-km DGG for a particular application or not. The effect of interpolating to a chosen model grid with smaller spatial resolution is also assessed. These questions are addressed through the use of high-resolution T_b observations from the Australian Airborne Cal/Val Experiment for SMOS (AACES) [7]. The AACES data cover the Murrumbidgee Catchment in southeastern Australia with diverse climatic and varying physiographic conditions. The high-resolution AACES data offer the capability to explore the representativeness of T_b at a variety of spatial resolutions and thus determine the level of uncertainty associated with using T_b observations made at one resolution and applied at another. Specifically, the results quantify the level of uncertainty expected when applying the following: 1) 42-km SMOS T_b observations on the 15-km DGG and 2) the subsequent interpolation of this 15-km T_b representation to a 12-km model grid. The possibility to flag times and/or locations when larger than acceptable errors are expected is also examined using three factors: 1) spatial variance of SMOS Level 1 observations; 2) density of vegetation cover; and 3) topography.

Manuscript received November 10, 2012; revised March 8, 2013; accepted April 5, 2013. This work was supported by the Australian Research Council under Grant DP0879212.

The authors are with the Department of Civil Engineering, Monash University, Melbourne, Vic. 3800, Australia (e-mail: dgiftman@hotmail.com; jeff.walker@monash.edu; chris.rudiger@monash.edu).

Color versions of one or more of the figures in this paper are available online at <http://ieeexplore.ieee.org>.

Digital Object Identifier 10.1109/TGRS.2013.2262501

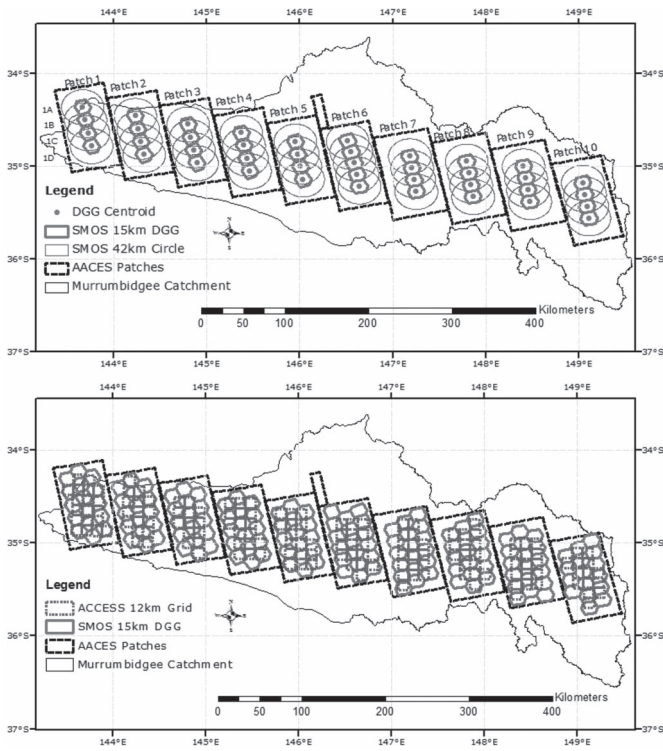


Fig. 1. Murrumbidgee Catchment study area showing the AACES flight patches, the SMOS 15-km DGG, and 42-km footprints (circles) that they represent. The bottom panel also shows the 12-km ACCESS model grid. Flight patch numbering starts with 1 at the left to 10 at the right. The DGG is labeled according to the flight patch number and alphabetic character starting with “A” at the top grid to “D” at the bottom grid except for patch 6 whose bottom grid is “E.”

II. MATERIALS AND METHODS

A. Study Area and T_b Data

The 80 000-km² Murrumbidgee Catchment shown in Fig. 1 has varied climatic, topographic, and land-cover characteristics with semi-arid conditions in the west to alpine conditions (including wintertime snow) in the east. The AACES campaign was undertaken in 2010 across the Murrumbidgee Catchment including AACES-1 in the summer and AACES-2 in the winter [7]. AACES-1 commenced on January 18 and was completed on February 21, whereas AACES-2 was undertaken from September 8 to 26. The airborne radiometer data cover a 500 × 100 km² area which is composed of the ten flight patches shown in Fig. 1, each being 50 × 100 km². The flight patches are aligned with the SMOS 15-km DGG; each patch contains a minimum of four overlapping SMOS pixels of about 42-km resolution. The microwave radiometer used is the Polarimetric L-band Multibeam Radiometer (PLMR) at 1.413-GHz frequency (the same frequency as in SMOS), which was mounted such that it scanned the surface at three incidence angles of ±7°, ±21.5°, and ±38.5° to each side of the aircraft. The PLMR used to make the 1-km T_b observations has an accuracy better than 2 K with sensitivity better than 1 K [8]. As a result, the uncertainty associated with the 1-km AACES T_b is taken to be 2 K.

The AACES data used in this study include the 1-km L-band T_b data normalized to a common 38° incidence angle to simulate a single incidence angle of SMOS Level 1 T_b

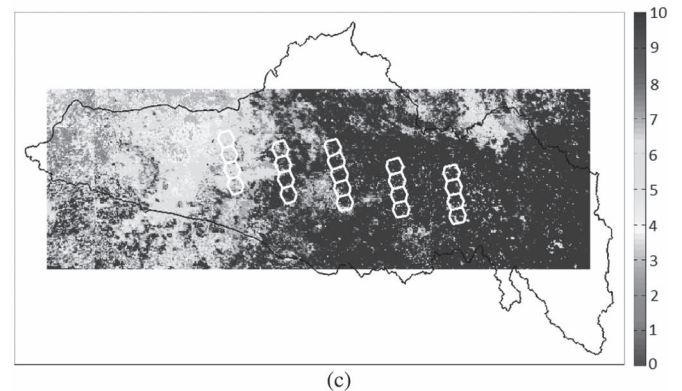
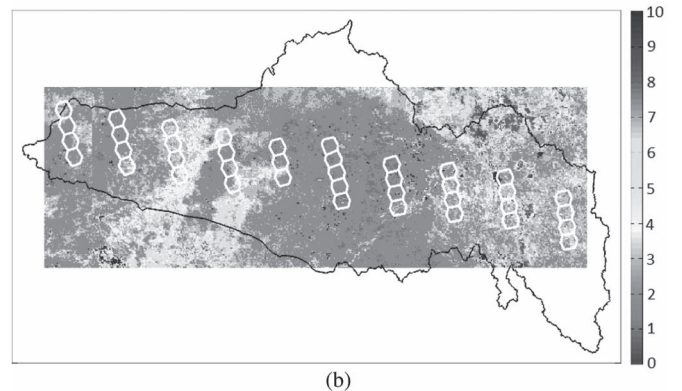
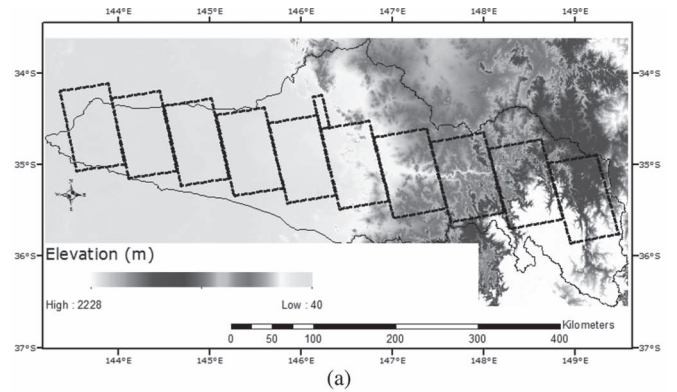


Fig. 2. Topographic information and density of vegetation cover in the Murrumbidgee Catchment during AACES observations (data source: DEM—Geoscience Australia; MODIS LAI-NASA LP DAAC at https://lpdaac.usgs.gov/get_data). (a) Terrain elevation showing smooth topographic roughness in the west to high topographic roughness in the east. (b) MODIS LAI in square meters per square meter during AACES-1 from January 18 to February 21. (c) MODIS LAI in square meters per square meter during AACES-2 from September 8 to 26.

data. The actual SMOS Level 1 T_b observations at about 38° incidence angle are only used in this study to examine the spatial variability of T_b as represented by SMOS data on the DGG within a single SMOS footprint. The reason for this reliance on the AACES data is the high resolution that it affords, allowing the questions of spatial resolution and interpolation to be fully addressed.

B. Topography and Vegetation Cover

The topography and the density of vegetation cover in the Murrumbidgee Catchment are shown in Fig. 2. The topography is represented through digital elevation model (DEM) data,

obtained from Geoscience Australia through the GEODATA 9 Second DEM (DEM-9S) Version 3 in 2008. The DEM has a spatial resolution of 250 m with a positional accuracy (in nominal scale) of 1:250 000. The topography in AACES patches 1–5 is flat, indicating low topographic roughness with patch 6 having gently sloping terrain and patches 7–10 have undulating terrain indicative of high topographic roughness. The density of vegetation cover is approximated using leaf area index (LAI) data in square meters per square meter from the 1-km Moderate-Resolution Imaging Spectroradiometer (MODIS) data. The LAI information on January 25 and September 13, 2010 are used to represent the density of vegetation cover during the AACES-1 and AACES-2 observation periods, respectively. Generally, the density of vegetation cover is less during AACES-1 compared with that during the AACES-2 observation period. The density of vegetation cover is highest at the eastern portion of the catchment, which comprises conservation areas and state forests, whereas the western areas are characterized mainly with grassland. It is noteworthy that the moderate densities of vegetation cover during AACES-1 around patches 3–4 in the central portion of the catchment are cropping irrigation areas.

C. Application Methods

The evaluation of T_b observations for the two spatial resolutions and interpolation onto a model grid is divided into three parts: A, B, and C. Part A examines the differences in T_b when 1-km AACES data are aggregated according to the 15-km DGG as compared with the 1-km AACES data aggregated for the actual 42-km footprint that it represents. Hereafter, the 1-km AACES data are denoted as $T_b^{1 \text{ km}}$, the aggregations to 15-km DGG as $T_b^{15 \text{ km}}$, the aggregations to 42 km as $T_b^{42 \text{ km}}$, and the use of $T_b^{42 \text{ km}}$ data as if they were the true $T_b^{15 \text{ km}}$ values as $T_b^{42/15 \text{ km}}$. The aggregations are performed by finding the average of all $T_b^{1 \text{ km}}$ grids that are contained within each of the 15-km DGG using (1) and in the actual 42-km SMOS footprint according to (2). The associated uncertainties for $T_b^{15 \text{ km}}$ and $T_b^{42 \text{ km}}$ are estimated using (3) and (4), respectively, derived according to the standard error propagation procedure [9] under the assumption that the error of each measurement is independent. This assumption is appropriate, given the nature of the errors in individual PLMR measurements and the application of the T_b data herein

$$T_b^{15 \text{ km}} = \frac{\sum_{i=1}^k T_{b,i}^{1 \text{ km}}}{k} \quad (1)$$

where k is the number of 1-km grids within the 15-km grid

$$T_b^{42 \text{ km}} = \frac{\sum_{i=1}^n T_{b,i}^{1 \text{ km}}}{n} \quad (2)$$

where n is the number of 1-km grids within the 42-km grid

$$\sigma_{T_b^{15 \text{ km}}} = \sqrt{\sum_{i=1}^k \left(\frac{\sigma_{T_{b,i}^{1 \text{ km}}}^2}{k^2} \right)} \quad (3)$$

where $\sigma_{T_b^{1 \text{ km}}}$ is the uncertainty from the 1-km T_b ($\approx 2 \text{ K}$)

$$\sigma_{T_b^{42 \text{ km}}} = \sqrt{\sum_{i=1}^n \left(\frac{\sigma_{T_{b,i}^{1 \text{ km}}}^2}{n^2} \right)}. \quad (4)$$

Using $T_b^{15 \text{ km}}$ for the 15-km DGG and $T_b^{42 \text{ km}}$ for the actual 42-km SMOS footprint, the differences in T_b between the two spatial resolutions provide an estimate of the uncertainty when applying the 42-km SMOS data directly on the 15-km DGG as $T_b^{42/15 \text{ km}}$. The absolute difference in T_b between the 15-km DGG and the actual 42-km SMOS footprint, referred to hereafter as T_b^{42-15} , is estimated in (5) and the associated uncertainty of this difference, denoted as $\sigma_{T_b^{42-15}}$, is determined according to (6)

$$T_b^{42-15} = |T_b^{42 \text{ km}} - T_b^{15 \text{ km}}| \quad (5)$$

$$\sigma_{T_b^{42-15}} = \sqrt{(\sigma_{T_b^{42 \text{ km}}})^2 + (\sigma_{T_b^{15 \text{ km}}})^2}. \quad (6)$$

The rationale of this evaluation is to determine the level of uncertainty in T_b when the actual 42-km SMOS observations are approximated to the 15-km DGG. Knowledge of the uncertainty in $T_b^{42/15 \text{ km}}$ will potentially allow practitioners to use the 42-km SMOS T_b observations directly at the 15-km DGG.

Part B assesses the uncertainty when interpolating the 15-km DGG T_b to model grids with geometry and resolution that are different to the DGG or the data-thinned original 42-km resolution. The model grid used in this study is a 12-km square grid which represents the numerical weather prediction grid from the Australian Community Climate and Earth-System Simulator (ACCESS). Consequently, two estimates of T_b are required for the 12-km model grid: one as a direct aggregation of the 1-km AACES data onto the 12-km resolution, hereafter referred to as $T_b^{12 \text{ km}}$, and the other as a weighted sum of the 15-km DGG T_b according to the areal overlaps with the 12-km resolution, hereafter referred to as $T_b^{w12 \text{ km}}$. The aggregated estimate $T_b^{12 \text{ km}}$ is determined by finding the average of the 1-km AACES data that are contained within the 12-km grid according to (7) with its associated uncertainty $\sigma_{T_b^{12 \text{ km}}}$ in (8) under the assumption of independence

$$T_b^{12 \text{ km}} = \frac{\sum_{i=1}^m T_{b,i}^{1 \text{ km}}}{m} \quad (7)$$

where m is the number of 1-km grids within the 12-km grid

$$\sigma_{T_b^{12 \text{ km}}} = \sqrt{\sum_{i=1}^m \left(\frac{\sigma_{T_{b,i}^{1 \text{ km}}}^2}{m^2} \right)} \quad (8)$$

where $\sigma_{T_b^{1 \text{ km}}}$ is the uncertainty from the 1-km T_b .

Since the PLMR coverage is not sufficiently large to provide the $T_b^{42/15 \text{ km}}$ values required by the 15-km DGG represented in the bottom panel of Fig. 1, only the actual 15-km DGG observations $T_b^{15 \text{ km}}$ could be used for explicit representation of the DGG and thus provide an estimate of $T_b^{12 \text{ km}}$ (denoted as $*T_b^{w12 \text{ km}}$) when using (9). While the difference between these two values ($T_b^{12 \text{ km}}$ and $*T_b^{w12 \text{ km}}$) provides an estimate of the error from interpolation itself and not the scaling error

that comes from using SMOS data directly on the DGG; error propagation on the interpolation equation in (9) will provide the theoretical error estimate.

The weighted 12-km estimate $*T_b^{w12 \text{ km}}$ is calculated according to (9) as a weighted sum by area (in terms of fractional coverage) for each 12-km grid using the 42-km observation on the 15-km grid [$T_b^{42/15 \text{ km}}$ from (2)]. The corresponding uncertainty estimate for $*T_b^{w12 \text{ km}}$ denoted as $*\sigma_{T_b^{w12 \text{ km}}}$ is estimated according to (10) from the standard error propagation procedure [9]. The estimate of the error from applying 42-km observations at 15-km DGG resolution, denoted as $\sigma_{T_b^{42/15 \text{ km}}}$, is taken as the root mean square difference (RMSD) for the difference calculated in (5)

$$*T_b^{w12 \text{ km}} = \sum_{i=1}^p \left(w_i * T_{b,i}^{42/15 \text{ km}} \right) \quad (9)$$

where p is the number of 15-km grids which overlap the 12-km grid, $w = A_{15 \text{ km}}^*/A_{12 \text{ km}}$, $A_{15 \text{ km}}^*$ is the area of the 15-km grid which overlaps with the 12-km grid, and $A_{12 \text{ km}}$ is the total area of the 12-km grid

$$*\sigma_{T_b^{w12 \text{ km}}} = \sqrt{\sum_{i=1}^m \left(w_i^2 * \sigma_{T_{b,i}^{42/15 \text{ km}}}^2 \right)}. \quad (10)$$

The weighted 12-km estimate and its error estimate from the actual 15-km data, denoted as $*T_b^{w12 \text{ km}}$, can be calculated from (9) and (10) by using $T_b^{15 \text{ km}}$ in place of $T_b^{42/15 \text{ km}}$ and $\sigma_{T_b^{15 \text{ km}}}$ from (3) in place of $\sigma_{T_{b,i}^{42/15 \text{ km}}}$.

Part C is an attempt to identify when and/or where it is more appropriate to approximate the 42-km SMOS T_b data on the 15-km DGG. This includes an evaluation of the differences in T_b between the observed 15-km resolution and the actual observation at 42 km in comparison with three factors: 1) the spatial variance of SMOS Level 1 data, 2) the density of vegetation cover, and 3) topographic roughness. The spatial variance of SMOS data is determined for each 15-km DGG by using its T_b value and the values from neighboring DGGs which fall within the 42-km SMOS footprint. The computed variance of T_b provides a measure of variability for the overlapping SMOS observations. The density of vegetation cover is represented using MODIS LAI by finding the average of all the 1-km LAI within each of the 42-km SMOS pixels.

The topographic roughness for each of the 42-km SMOS pixels is estimated using the DEM data. The derived terrain slope angles from the DEM were used to estimate a topographic indicator as an absolute value of the product of spatial variance and skewness of the slope angle. This topographical indicator is denoted as $sVar$ and provides an index of both the heterogeneity (variance) and uniformity (skewness) of the landscape [10]. It is noteworthy that $sVar$ is a relative measure that is meaningful only for a particular defined area. High values of $sVar$ indicate that the terrain is nonuniformly heterogeneous, low values mean a uniformly homogeneous terrain, and moderate values mean that the terrain is either uniformly heterogeneous or nonuniformly homogeneous. These comparisons are aimed to determine whether the pattern of uncertainty found between

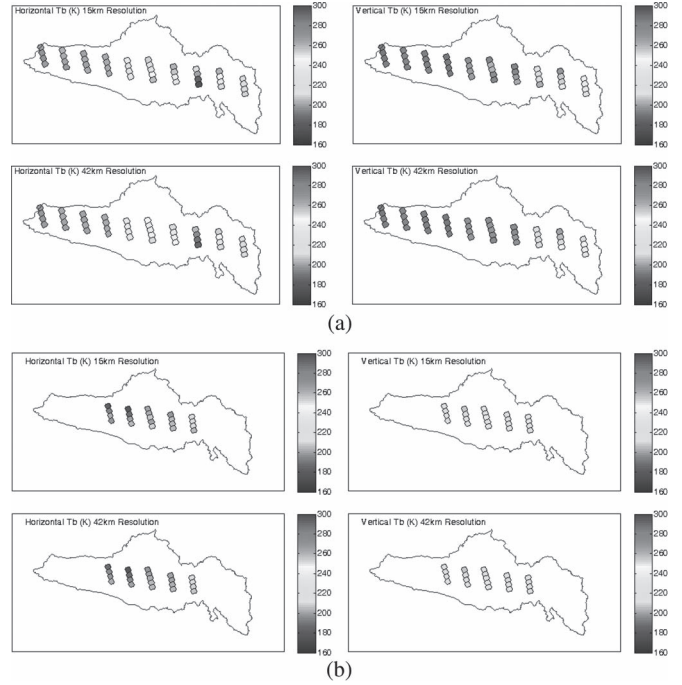


Fig. 3. Brightness temperature in kelvin; observed 1-km AACES T_b aggregated to the 15-km DGG and to the actual 42-km SMOS footprint that is represented on the 15-km DGG. (a) AACES-1: Patch numbering starts from 1 at far left to 10 at far right. (b) AACES-2: Patch numbering starts from 4 at far left to 8 at far right.

the 15-km DGG representation and the actual 42-km SMOS footprint corresponds to the spatial variability in the SMOS data, vegetation cover, or topographic roughness.

III. RESULTS AND DISCUSSION

A. Variability of Aggregated T_b for Actual 42-km SMOS Footprint and 15-km DGG

The aggregated T_b values for the 15- and 42-km resolutions are presented in Fig. 3 for AACES-1 and AACES-2. In AACES-1, larger differences between the two resolutions can be seen in patches 8–10 (relatively wet conditions) whereas the remaining patches show little discernible differences for H and V polarizations. In AACES-2, the T_b differences for the two resolutions are minimal and limited to a few DGG pixels in both polarizations. It is noteworthy that in AACES-1, surface soil moisture obtained from *in situ* point observations varied considerably from dry conditions of $0.05\text{--}0.10 \text{ m}^3/\text{m}^3$ for the left patches (1–4) to wet conditions of $0.25\text{--}0.35 \text{ m}^3/\text{m}^3$ for the right patches (5–10), whereas consistent wet conditions of $0.2\text{--}0.4 \text{ m}^3/\text{m}^3$ persisted for all patches observed during AACES-2 [7].

The overall quantitative comparison between the two resolutions is shown in Fig. 4. Note that T_b values are generally low for AACES-2, reflecting the wetter conditions and lower surface temperatures prevailing during this winter campaign, whereas AACES-1 has values spread over the entire interval, reflecting the more varied soil moisture conditions. However, the pattern of differences in T_b between the two resolutions is similar for AACES-1 and AACES-2, as evidenced by their RMSD and R^2 . The RMSD between the two T_b estimates is 4.5 K in the H polarization and 3.9 K in the V polarization.

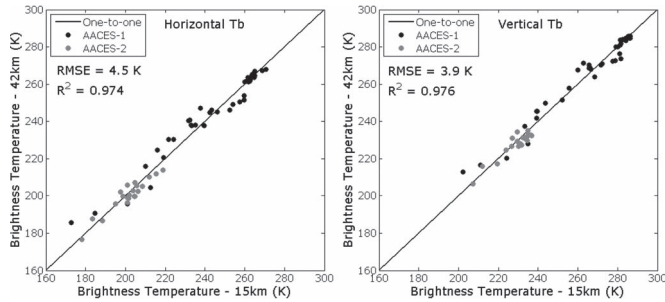


Fig. 4. Comparison between the aggregated T_b at 15- and 42-km resolutions, as shown in Fig. 3. The estimated T_b errors according to (3) and (4) are 0.2 K for $T_b^{15\text{ km}}$ and 0.1 K for $T_b^{42\text{ km}}$ under the assumption of independence. If dependence was assumed, then these would each increase to the original 2-K uncertainty of PLMR.

While the results show that the highest T_b values, indicative of extreme dry locations, have an almost perfect match between the two resolutions in both polarizations, the T_b comparison between the two resolutions does not significantly degrade for T_b values. Thus, the T_b differences shown here do not seem to be strongly correlated with soil moisture (dry or wet). Rather, the closer agreement at the extreme dry locations is, in general, due to the homogeneous nature (e.g., vegetation cover and physiographic heterogeneity) of the landscape, together with uniform soil moisture conditions over large areas. The terrain and vegetation density are much more heterogeneous in the eastern portion of the catchment, indicating that these locations are likely to have more dynamic and nonuniform moisture conditions. As will be shown later, the lowest absolute differences in T_b between the two resolutions are all located in patches 1–4, being the western portion of the catchment.

B. Variability of T_b Between Aggregated 12-km and Weighted 12-km Model Grids

The aggregated 12-km T_b and its weighted estimate using the observed 15-km T_b are shown in Fig. 5, with very little difference between the two T_b estimates for both polarizations across AACES-1 and AACES-2. The quantitative comparison for the two 12-km estimates is shown in Fig. 6. This confirms the similarity in pattern with a coefficient of determination (R^2) of about 0.98 in both polarizations. The RMSD value between the two T_b estimates is 4.0 K in the H polarization and 3.6 K in the V polarization. However, as noted earlier, this comparison only represents the error introduced by interpolating from the 15-km DGG to the 12-km grid and does not account for the error of SMOS data representation on the 15-km DGG. Due to the limitations of the available data set, this can only be estimated from error proration calculation and not by direct deduction.

By using the RMSD values from Part A as estimates of uncertainty in the T_b data on the 15-km DGG (i.e., $\sigma_{T_b^{42/15}}$), the overall uncertainty in T_b associated with interpolating the 42-km SMOS data to the 12-km model grid can be calculated from (10) as 3.3 K in the H polarization and 2.9 K in the V polarization under the assumption of independence. However, under the assumption of dependence, the uncertainty estimates would remain as 4.5 K in the H polarization and 3.9 K in the V polarization. Alternatively, assuming additive errors, the error in interpolating the 42-km SMOS data onto the 12-km grid can

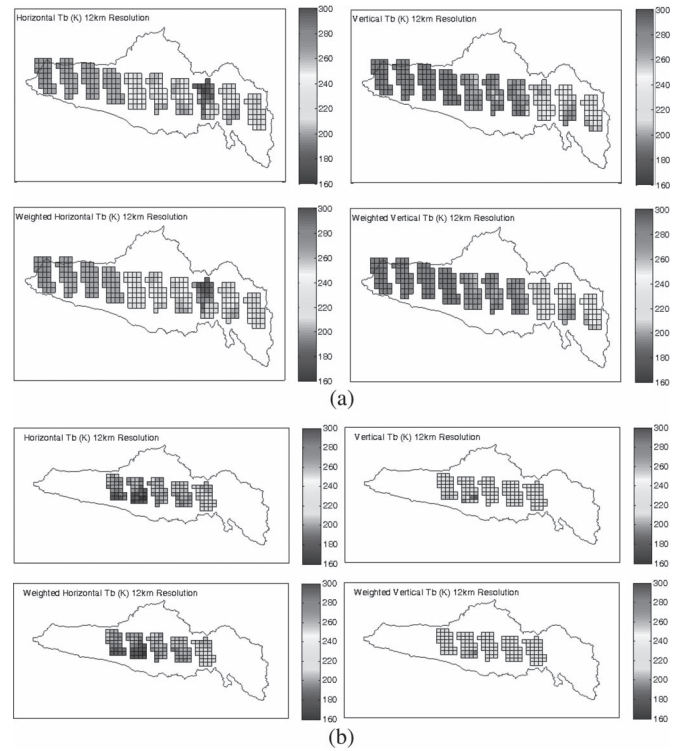


Fig. 5. Brightness temperature in kelvin; observed 1-km AACES T_b aggregated to the 12-km model grid and the weighted 12-km T_b estimated as the weighted sum of 15-km T_b as in Fig. 3. (a) AACES-1: Patch numbering starts from 1 at far left to 10 at far right. (b) AACES-2: Patch numbering starts from 4 at far left to 8 at far right.

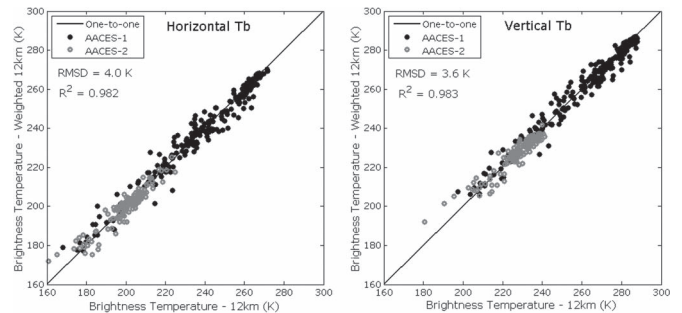


Fig. 6. Comparison between observed 1-km AACES T_b aggregated to the 12-km T_b and the weighted 12-km T_b estimated as the weighted sum of aggregated 15-km T_b , as shown in Fig. 5. The associated T_b errors according to (8) and (10) (using $T_b^{15\text{ km}}$) are 0.2 K for $T_b^{12\text{ km}}$ and 1.8 K for $T_b^{w12\text{ km}}$ under the assumption of independence. If dependence was assumed, then these would each increase to the original 2-K uncertainty of PLMR.

be estimated as $\sqrt{(4.5)^2 + (4.0)^2} = 6.0$ K in the H polarization and $\sqrt{(3.9)^2 + (3.6)^2} = 5.3$ K in the V polarization.

C. Indicators for Estimating T_b Differences Between 15- and 42-km Resolutions

This section presents the differences in T_b between the 15-km DGG and the 42-km SMOS footprint in comparison with the three indicators: spatial variance of SMOS Level 1 data, vegetation cover, and topography. Using T_b differences between the 15- and 42-km resolutions, the spatial variance of actual SMOS observations are compared with the absolute differences from Part A. The variance for each SMOS DGG is computed by finding the standard deviation of T_b using values from the

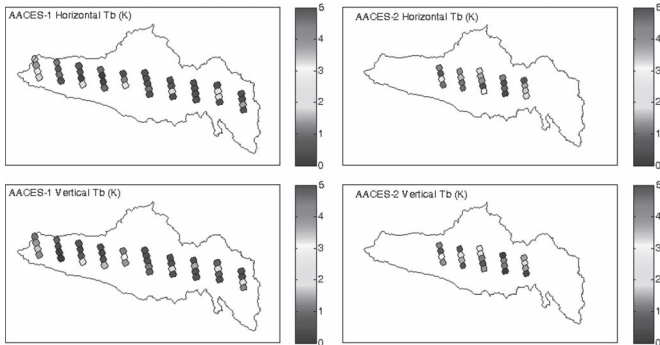


Fig. 7. Brightness temperature in kelvin; absolute difference of T_b between observed 1-km AACES T_b aggregated to the 42-km SMOS footprint and the actual observations for the 15-km DGG, as shown in Fig. 3.

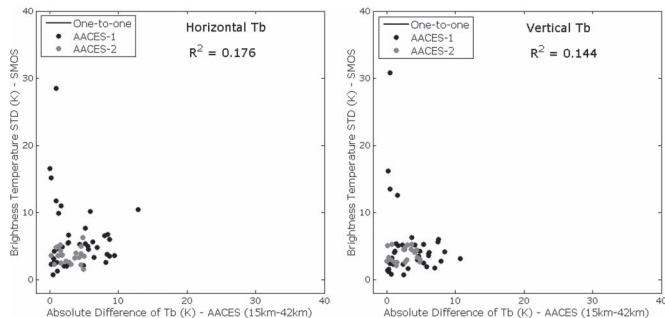


Fig. 8. Comparison between standard deviation of actual SMOS T_b observations within a given footprint and the absolute difference of T_b shown in Fig. 7. The R^2 values are computed after removing SMOS standard deviation and AACES absolute values greater than 10 K.

footprint in question and the six other neighboring DGG values that fall within it. This comparison of the actual T_b standard deviation with the absolute difference provides a mechanism to determine if any relationship exists to identify places and/or times when the difference in T_b is expected to exceed a given tolerance. The absolute difference of T_b between the 42- and 15-km resolutions is shown in Fig. 7.

Generally, the smaller absolute differences occur in patches 1–4 in the western portion of the catchment, as shown previously to have smooth topographical roughness. The figure identifies (by deep brown shading) grids with absolute differences greater than the overall RMSD values of 4.6 K for H polarization and 3.9 K for V polarization in Part A; note that the grid labels have been defined earlier in Fig. 1. These grids (in patches 5–10) are generally located in the eastern portion having heterogeneous physiographic conditions of the catchment. The grids in patches 7 and 8 (e.g., 7B and 8A) have consistently high absolute differences for both V and H polarizations in AACES-1 and AACES-2. Patches 9 and 10 also have high absolute differences in V and H polarizations in AACES-1. The persistent pattern in these grids suggests that they are associated with unique physiographic/observation features.

The computed standard deviation using actual SMOS Level 1 T_b for the grids are compared with the T_b absolute difference in Fig. 8 for both H and V polarizations. The estimated standard deviation values are generally below 10 K, but four isolated grids have high variance values ranging from above 10 K to 30 K. These high standard deviation values are generally found in patch 4, which has extensive but scattered crop irrigation ar-

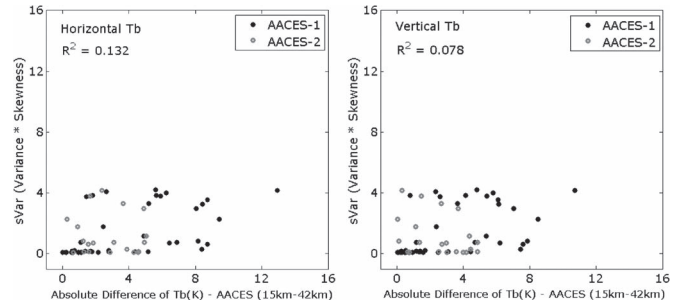


Fig. 9. Comparison between topographical roughness $sVar$ and the absolute difference of T_b shown in Fig. 7.

eas. The overall pattern of the T_b standard deviation is unrelated to dry or wet locations in the Murrumbidgee Catchment. Based on the R^2 values, there is only a weak relationship between the standard deviation of SMOS Level 1 T_b and the absolute difference computed using 42- and 15-km resolutions.

The absolute difference of T_b for the two resolutions was also examined in relation to topographic roughness and vegetation cover using LAI. It was found from the LAI data that there are different densities of vegetation cover during the two field campaigns, yet the absolute differences of T_b are similar for the two seasons. As a result, the absolute differences in T_b between the 15-km DGG and actual 42-km SMOS footprint do not correlate to the density of vegetation cover.

For topography, the varied terrain pattern indicative of high topographic roughness at the eastern portion of the Murrumbidgee Catchment is consistent with the high absolute differences of T_b in patches 5–10. The impact of topography is examined by comparing the topographical index $sVar$ with the absolute differences of T_b in Fig. 9. The $sVar$ pattern shows a weak relationship (based on the R^2 values) with the absolute differences of T_b in both H and V polarizations.

Overall, the topography, vegetation, and spatial variance of SMOS Level 1 data show weak relationships to the absolute differences in T_b . Given these findings, none of the three indicators evaluated was able to identify where (i.e., spatial locations) and when (e.g., days or seasons) the differences in T_b for 15- and 42-km resolutions will be large or small.

IV. CONCLUSION

This study has applied 1-km T_b data from AACES to examine the potential error from using the 15-km DGG to represent T_b observations at the actual 42-km SMOS footprint and subsequent interpolation to a 12-km model grid. The evaluation shows that the overall differences in T_b based on RMSD between the 15-km DGG and the actual 42-km footprint are about 4.5 K and 3.9 K for H and V polarizations, respectively. The pattern of differences in T_b show that larger absolute differences were associated with heterogeneous physiographic areas whereas smaller differences were related to homogeneous areas with low topographic roughness of the catchment. As a result, the differences in T_b were further examined in relation to three features: the spatial variance of SMOS Level 1 data, vegetation cover, and topographic roughness. However, only poor relationships were found with these three indicator variables.

When interpolating SMOS T_b data from the 15-km DGG to a 12-km regular grid, results showed that the overall differences in T_b between aggregated 12-km and weighted 12-km from the 15-km observation were 4.0 K and 3.6 K for H and V polarizations, respectively. By taking into account the T_b error in representing the 42-km SMOS footprint directly on the 15-km DGG, together with the interpolation from the 12-km resolution, the overall error from 42- to 12-km resolution was estimated to be between 3.3 K and 4.5 K in the H polarization and between 2.9 K and 3.9 K in the V polarization according to the assumption made in relation to dependence. The independent combination of the T_b errors associated with the two interpolations shows T_b uncertainties of 6 K and 5.3 K in the H and V polarizations, respectively.

This evaluation of differences in T_b between the actual 42-km footprint and the 15-km DGG provides an estimate of the uncertainty to be expected for similar physiographic regions when applying SMOS data directly on the DGG. Given the estimated errors, the SMOS T_b observations at 42 km can be used directly on the DGG without downscaling procedures, as the expected RMSD is not worse than the noise that currently exists in SMOS T_b measurements. That is, soil moisture retrieval and data assimilation applications can use the 42-km SMOS T_b observations on the 15-km DGG without downscaling since the estimated errors in T_b between the two resolutions are smaller than the standard error of the current SMOS T_b data.

ACKNOWLEDGMENT

The authors would like to thank all participants in both AACES campaigns, the anonymous reviewers for their comments, and the Editor for handling the manuscript.

REFERENCES

- [1] Y. Kerr, P. Waldteufel, J.-P. Wigneron, S. Delwart, F. Cabot, J. Boutin, M.-J. Escorihuela, J. Font, N. Reul, C. Gruhier, S. Juglea, M. Drinkwater, A. Hahne, M. Martin-Neira, and S. Mecklenburg, "The SMOS mission: New tool for monitoring key elements of the global water cycle," *Proc. IEEE*, vol. 98, no. 5, pp. 666–687, May 2010.
- [2] O. Merlin, C. Rüdiger, A. Al Bitar, P. Richaume, J. Walker, and Y. Kerr, "Disaggregation of SMOS soil moisture in Southeastern Australia," *IEEE Trans. Geosci. Remote Sens.*, vol. 50, no. 5, pp. 1556–1571, May 2012.
- [3] M. Piles, A. Camps, M. Vall-llossera, I. Corbella, R. Panciera, C. Rüdiger, Y. Kerr, and J. Walker, "Downscaling SMOS-derived soil moisture using MODIS visible/infrared data," *IEEE Trans. Geosci. Remote Sens.*, vol. 49, no. 9, pp. 3156–3166, Sep. 2011.
- [4] M. Pan and E. F. Wood, "Impact of accuracy, spatial availability, and revisit time of satellite-derived surface soil moisture in a multiscale ensemble data assimilation system," *IEEE J. Sel. Topics Appl. Earth Observ. Remote Sens.*, vol. 3, no. 1, pp. 49–56, Mar. 2010.
- [5] W. T. Crow and D. Ryu, "A new data assimilation approach for improving runoff prediction using remotely-sensed soil moisture retrievals," *Hydrol. Earth Syst. Sci.*, vol. 13, no. 1, pp. 1–16, Jan. 2009.
- [6] R. H. Reichle, W. T. Crow, R. D. Koster, H. O. Sharif, and S. P. P. Mahanama, "Contribution of soil moisture retrievals to land data assimilation products," *Geophys. Res. Lett.*, vol. 35, no. 1, p. L01404, Jan. 2008.
- [7] S. Peischl, J. P. Walker, C. Rüdiger, N. Ye, Y. H. Kerr, E. Kim, R. Bandara, and M. Allahmoradi, "The AACES field experiments: SMOS calibration and validation across the Murrumbidgee River catchment," *Hydrol. Earth Syst. Sci.*, vol. 16, no. 6, pp. 1697–1708, Jun. 2012.
- [8] J. P. Grant, A. A. Van de Griend, J.-P. Wigneron, K. Saleh, R. Panciera, and J. P. Walker, "Influence of forest cover fraction on L-band soil moisture retrievals from heterogeneous pixels using multi-angular observations," *Remote Sens. Environ.*, vol. 114, no. 5, pp. 1026–1037, May 2010.
- [9] P. Fornasini, *The Uncertainty in Physical Measurements: An Introduction to Data Analysis in the Physics Laboratory*. New York, NY, USA: Springer-Verlag, 2008.
- [10] V. Guttal and C. Jayaprakash, "Spatial variance and spatial skewness: Leading indicators of regime shifts in spatial ecological systems," *Theor. Ecol.*, vol. 2, no. 1, pp. 3–12, Mar. 2009.



Gift Dumedah received the B.Sc. degree (with honors) in geodetic engineering from Kwame Nkrumah University of Science and Technology, Kumasi, Ghana, in 2002 with his thesis entitled "A Geographical Information System for the Ghana Army." He also received the M.Sc. degree in geography from Simon Fraser University, Vancouver, BC, Canada, in 2005, with a specialization in geographic information science, and the Ph.D. degree in geography from the University of Guelph, Guelph, ON, Canada, in 2010, with his thesis titled "Multi-Objective

Calibration of Hydrological Models and Data Assimilation Using Genetic Algorithms."

After his studies, he held a postdoctoral fellowship at the School of Geography and Earth Sciences, McMaster University, Hamilton, ON, Canada. In October 2011, he joined the Department of Civil Engineering, Monash University, Melbourne, Australia, where he is currently contributing to soil moisture research for sustainable land and water management. His research focus is on the integrated assessment of climate variability and human impact on sustainable water resources by employing advanced land surface monitoring strategies for efficient observation–model synthesis. His specific primary interests include observation–model synthesis, data assimilation, evolutionary computation, and remote sensing and GIScience applied to water resources.

Jeffrey P. Walker received the B.E. degree (with Honours 1 and University Medal) in civil engineering and B.S. degree in surveying (with Honours 1 and University Medal) and the Ph.D. degree in water resources engineering from The University of Newcastle, Newcastle, Australia, in 1995 and 1999, respectively. His Ph.D. thesis was among the early pioneering research on estimation of root-zone soil moisture from remotely sensed surface soil moisture observations.

He then joined the NASA Goddard Space Flight Center to implement his soil moisture work globally. In 2001, he moved to the Department of Civil and Environmental Engineering, The University of Melbourne, Melbourne, Australia, as a Lecturer, where he continued his soil moisture work, including the development of the only Australian airborne capability for simulating new satellite missions for soil moisture. Since 2010, he has been a Professor with the Department of Civil Engineering, Faculty of Engineering, Monash University, Melbourne, where he is continuing his research. He is contributing to soil moisture satellite missions at NASA, the European Space Agency, and JAXA as a Science Definition Team Member for the Soil Moisture Active Passive Mission and a Calibration/Validation Team Member for the Soil Moisture and Ocean Salinity mission.

Christoph Rüdiger (M'10) received the B.E. degree in civil engineering from the University of Applied Sciences of Wiesbaden, Wiesbaden, Germany, in 2002 and the Ph.D. degree in environmental engineering from The University of Melbourne, Melbourne, Australia, in 2007. His undergraduate thesis covered the topic of groundwater and contaminant flow around future buildings. His Ph.D. thesis was on the potential to assimilate streamflow data into land surface models for soil moisture prediction.

He then joined the Centre National de Recherches Météorologiques, Météo, Toulouse, France, where he worked on the preparation of surface soil moisture and leaf-area-index data assimilation into the French land surface model ISBA. During this period, he also worked on the validation of different passive and active microwave satellite products over France with a particular focus on Soil Moisture and Ocean Salinity (SMOS). Since his return to Australia in July 2008, he has coordinated and led a number of calibration/validation (cal/val) campaigns for the Australian land validation segment of European Space Agency's SMOS mission in the Australian arid zone and the Murrumbidgee River catchment. In addition to this, he continues to work on land surface data assimilation and also participates in the Australian cal/val campaigns for the Soil Moisture Active Passive and the Aquarius missions. He is currently with Monash University, Melbourne.